Multidimensional nonlinear mirror-mode structures in the Earth's magnetosheath

Shoji, Masafumi; Omura, Yoshiharu; Lee, Lou-Chuang

JOURNAL OF GEOPHYSICAL RESEARCH, VOL. 117, A08208, doi:10.1029/2011JA017420, 2012

Multidimensional nonlinear mirror-mode structures in the Earth's magnetosheath

Masafumi Shoji,[1,2] Yoshiharu Omura,[1] and Lou-Chuang Lee[3]

Received 29 November 2011; revised 4 June 2012; accepted 17 June 2012; published 3 August 2012.

[1] We performed two-dimensional (2D) and three-dimensional (3D) hybrid simulations in open boundary models to study the nonlinear mirror-mode structures driven by the temperature anisotropy ($T_\perp/T_\parallel > 1$) of protons in the magnetosheath. In the open systems, because of the propagation of EMIC waves, we obtain the clearer non-propagating mirror-mode structures. We analyzed the relation between the mirror instability and the magnetic peaks and dips observed in the magnetosheath. In the 2D open boundary model with low beta ($\beta_\parallel \lesssim 1$), we obtain fine structures of the magnetic dips at the nonlinear stage. In the 3D model, on the other hand, the mirror instability makes the magnetic peak structures with the same parameters. The parametric analysis indicates that the magnetic peaks also arise in both 2D and 3D high beta cases ($\beta_\parallel \gtrsim 1$) as shown by the Cluster observations. In the high beta cases, the high mobility of the protons helps continuous coalescence of the diamagnetic currents inside the magnetic dips. The coalescence makes the magnetic dips larger and shallower. Between the large and shallow magnetic dips, the magnetic peaks appear in the high beta cases. In the 3D models, because degree of freedom increases in the perpendicular direction, the continuous coalescence can take place even in the low beta cases. Thus, the magnetic peaks appear in the 3D models in both cases.

Citation: Shoji, M., Y. Omura, and L.-C. Lee (2012), Multidimensional nonlinear mirror-mode structures in the Earth's magnetosheath, *J. Geophys. Res.*, *117*, A08208, doi:10.1029/2011JA017420.

1. Introduction

[2] The mirror instability is a well-known electromagnetic phenomenon which is excited by the temperature anisotropy ($T_\perp/T_\parallel > 1$) of hot ions in the perpendicular direction to the ambient magnetic field [*Vedenov and Sagdeev*, 1958; *Chandrasekhar et al.*, 1958; *Hasegawa*, 1969, 1975]. The associated mirror-mode structures are often observed in the magnetosheath of the Earth [e.g., *Tsurutani et al.*, 1982, 1984; *Hubert*, 1994; *Phan et al.*, 1994; *Lacombe and Belmont*, 1995], the planets [e.g., *Tsurutani et al.*, 1993; *Violante et al.*, 1995], the comets [*Tsurutani et al.*, 1999a; *Russell et al.*, 1989; *Glassmeier et al.*, 2003] and the heliosheath [*Tsurutani et al.*, 2011]. They are formed when the anisotropic hot ions satisfy the condition: $\beta_\perp/\beta_\parallel > 1 + 1/\beta_\perp$ [e.g., *Hasegawa*, 1969; *Price et al.*, 1986; *Lee et al.*, 1988; *Southwood and Kivelson*, 1993; *Kivelson and Southwood*, 1996], where $\beta_\perp$ and $\beta_\parallel$ are the ion beta values perpendicular and parallel to the background magnetic field. The mirror instability has the largest linear growth rate when the wave numbers directions become more oblique as the threshold excess of the instability increases [*Pokhotelov et al.*, 2004] and the frequency $\omega = 0$. Thus the mirror-mode structures do not move from the region where they arise.

[3] The temperature anisotropy also drives the L-mode electromagnetic ion cyclotron (EMIC) instability [*Kennel and Petschek*, 1966], which has a larger linear growth rate than that of the mirror instability [*Gary*, 1992; *Lacombe and Belmont*, 1995]. Comparing the L-mode EMIC and mirror instabilities in the multidimensional periodic boundary systems, we have shown that the mirror instability dominates over the L-mode EMIC instability in the Earth's magnetosheath [*Shoji et al.*, 2009]. We have found that one of the important points for the dominance of the mirror instability is the 3D spatial distributions of wave number spectra. The mirror-mode structures have wave number vectors mostly in the oblique directions and thus their wave number spectra become like a "torus". The difference of nonlinear evolutions of the L-mode EMIC waves and mirror-mode structures are also important because the L-mode EMIC waves cause the nonlinear wave-particle interactions, heat ions, and lose energy. As a result of the competition, only the mirror-mode structures remain in the space.

[4] Satellite observations [*Soucek et al.*, 2008; *Balikhin et al.*, 2009, 2010] indicate that the mirror-mode structures are observed as large amplitude quasiperiodic sinusoidal structures called magnetic peaks (also called humps) and magnetic dips (also called holes) in the terrestrial magnetosheath. *Soucek et al.* [2008] reported observations of

[1]Research Institute for Sustainable Humanosphere, Kyoto University, Uji, Japan.
[2]Now at Japan Aerospace Exploration Agency, Institute of Space and Astronautical Science, Sagamihara, Japan.
[3]Institute of Space Science, National Central University, Jhongli, Taiwan.

Corresponding author: M. Shoji, Japan Aerospace Exploration Agency, Institute of Space and Astronautical Science, 3-1-1 Yoshinodai, Chuoku, Sagamihara, Kanagawa 252-5210, Japan. (shoji@stp.isas.jaxa.jp)

0148-0227/12/2011JA017420

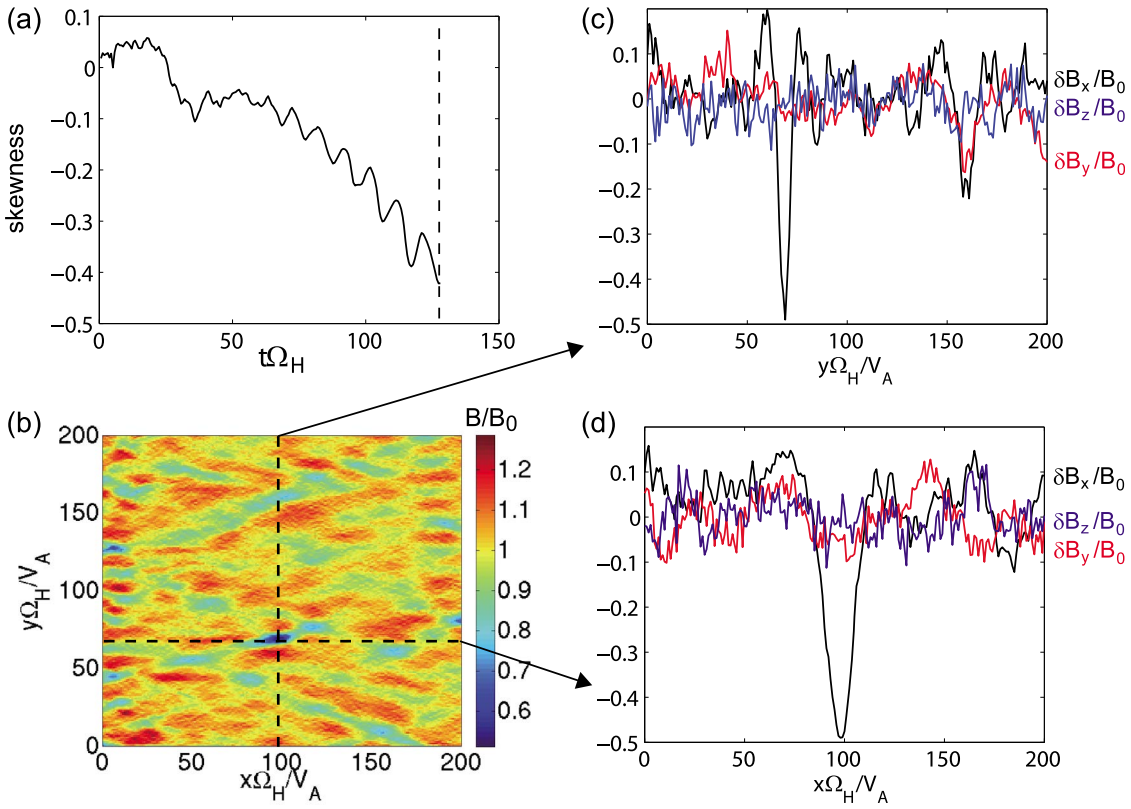

Figure 1. The skewness of δB_x and the typical magnetic structures in the 2D open boundary models with $T_\perp/T_\parallel = 4$ and $\beta_\parallel = 0.5$. (a) The skewness of δB_x calculated with whole grid points. (b) Contour of $B/B_0 = |\boldsymbol{B}_0 + \delta\boldsymbol{B}|/B_0$ at $t = 120/\Omega_H$ which is indicated by a dashed line in Figure 1a. (c, d) Waveforms of the magnetic field components along $y = 70\ V_A/\Omega_H$ and $x = 100\ V_A/\Omega_H$, which are shown by dashed lines in Figure 1b, respectively. In each panel, the black, red, and blue lines show $\delta B_x/B_0$, $\delta B_y/B_0$, and $\delta B_z/B_0$, respectively.

magnetic peaks near the bowshock and of the magnetic dips near the magnetopause. They also showed the dependence of magnetic structures on the temperature anisotropy and beta of ions. A one-dimensional hybrid simulation [*Califano et al.*, 2008] and quasi-linear theoretical analyses [*Hellinger et al.*, 2006] were performed. They show contributions of the nonlinear term of the mirror-mode structures to the magnetic peaks and dips.

[5] The torus-like wave number spectra in the 3D space also make magnetic structures different from those in the 2D space. The purpose of the present study is to understand how the spatial dimensionality affects the nonlinear mirror-mode structures. We also perform parametric analysis on the ion beta to explain the observational results that the magnetic dips appear in lower beta conditions [*Soucek et al.*, 2008]. Since the simulations just start from an initial velocity distribution in a uniform model, comparison of the temperature anisotropy and distance dependencies with the observation is difficult. Therefore, in this study, we concentrate on the ion beta dependency. In the present study, we perform the 2D and 3D hybrid simulations with open boundaries. In section 2, we briefly explain the model of the hybrid simulations. In section 3, we compare the 2D and 3D simulation results in the open boundary models with the same parameters. In section 4, the simulations with higher spatial resolution are performed. We discuss different evolutions of the mirror-mode structures in these models. The dependence on the ion beta is also discussed. Finally, we summarize the results in section 5.

2. Multidimensional Hybrid Code With Open Boundaries

[6] We developed the multidimensional (2D and 3D) hybrid code with open boundaries based on *Shoji et al.* [2009] in which the modified Current Advance Method and the Cyclic Leapfrog (CAM-CL) [*Matsumoto and Omura*, 1993] and the area sharing method to compute the ion current are used. We extended the 1D open boundary model [*Shoji and Omura*, 2011; *Shoji et al.*, 2011] to 2D and 3D models. The dumping layers [*Umeda et al.*, 2001] are set outside the physical region when the open boundary is selected. The three-point digital filter [*Birdsall and Langdon*, 1985] is applied to suppress current noise that can arise in high wave number space caused by lack of particles. In this code, we can select the periodic or open boundary in each direction. The transverse wave magnetic fields are dumped as

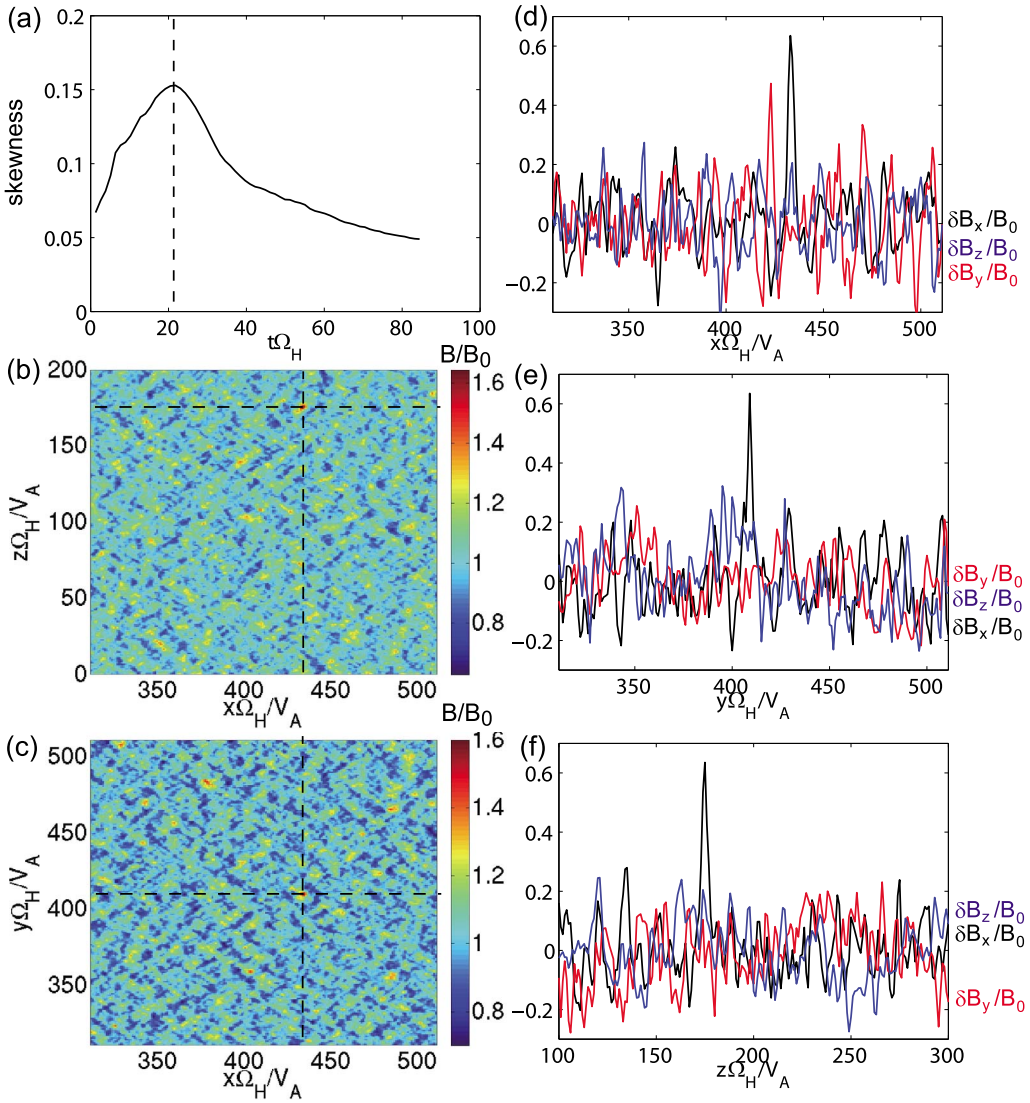

Figure 2. The skewness of δB_x and the typical magnetic structures in the 3D open boundary model with $T_\perp/T_\parallel = 4$ and $\beta_\parallel = 0.5$. (a) The skewness of δB_x calculated with whole grid points. (b, c) Cross sections of $B/B_0 = |\boldsymbol{B}_0 + \delta\boldsymbol{B}|/B_0$ at $t = 40\ \Omega_H$ which is indicated by a dashed line in Figure 2a in xz ($y = 410\ V_A/\Omega_H$) and xy ($z = 170\ V_A/\Omega_H$) plane. (d, e, f) Waveforms of the magnetic field components along $z = 170\ V_A/\Omega_H$ in Figure 2b, $y = 410\ V_A/\Omega_H$ in Figure 2c and $x = 430\ V_A/\Omega_H$ in Figure 2b, respectively. In each panel, the black, red, and blue lines show $\delta B_x/B_0$, $\delta B_y/B_0$, $\delta B_z/B_0$, respectively.

$B_{dump}(x) = r(x)B(x)$ at each time step, where $r(x)$ is the masking function defined as

$$r(x) = \begin{cases} 1 & (|x| \le X/2) \\ 1 - r_D \dfrac{(|x| - X/2)^2}{L_D^2} & (|x| > X/2) \end{cases}, \qquad (1)$$

where X is the size of the simulation space, L_D is the length of the damping region in each direction and $r_D = 0.12$ is a coefficient for the best dumping effect given by the experimental equation [*Umeda et al.*, 2001]. The number of the grids of the dumping layers for the open boundary is 32 in each end of the axis. Protons forming the bi-Maxwellian distribution are uniformly distributed in the simulation space. The plasma frequency of protons is $\omega_{pH} = 300\ \Omega_H$, where Ω_H is the proton gyrofrequency. A constant background magnetic field B_0 is assumed in the x direction. The electron beta is $\beta_e = 1.0$.

[7] We discuss the contribution of the mirror instability to the magnetic peaks or dips in the 2D and 3D models. We use the skewness (or called peakness in *Soucek et al.*, [2008]) to identify the magnetic structures as magnetic peaks or dips, which is introduced in *Califano et al.* [2008]. The skewness is a statistical value to measure an asymmetry of a distribution of samples. When the skewness is positive, the right tail of the distribution is longer than the left tail. In this case, the mass of the sample is concentrated on the left side. When

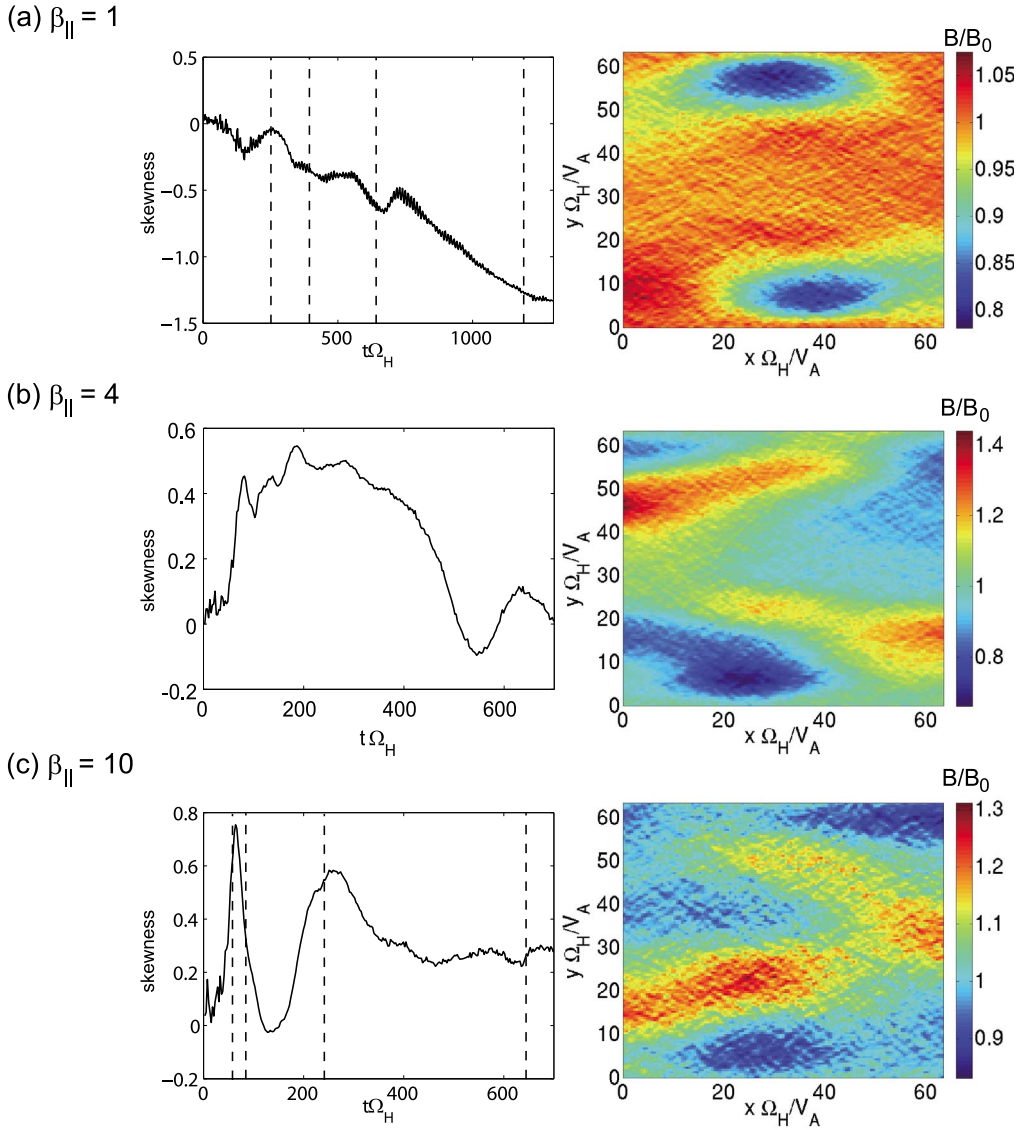

Figure 3. (left) Skewness of B_x and (right) Mirror-mode structures in the 2D model with the initial ion parameters $T_\perp/T_\parallel = 2$ and (a) $\beta_\parallel = 1$ at $t = 1308.6/\Omega_H$, (b) $\beta_\parallel = 4$ at $t = 652.8/\Omega_H$, and (c) $\beta_\parallel = 10$ at $t = 652.8/\Omega_H$.

the skewness is negative, the left tail is longer, the mass of the sample is concentrated on the right side. Applying this statistical analysis to the mirror-mode structure, we can find out whether the magnetic field slant on the left or right tails of the distribution. The positive skewness indicates magnetic peaks, while the negative one indicates magnetic dips. The skewness s for a set of sample values $\{s_k\}$ is defined as the normalized third momentum: $s = \mu_3/\sigma^3$, where μ_n is the nth momentum of the sample defined by $\mu_n = \frac{1}{N}\sum_{k=1}^{N}(x_k - m)^n$, ($m$ is the mean of $\{x_k\}$) and $\sigma = \sqrt{\mu_2}$ (standard deviation).

3. Nonlinear Structures in the Open Boundary Systems

[8] In a system with the periodic boundaries, the L-mode EMIC waves propagating along the parallel direction stay in the simulation space. We cannot neglect the effect of the L-mode EMIC instability such as formation of the nonlinear potentials by the forward and backward propagating EMIC waves [*Omura et al.*, 1988]. Especially, in the 2D model, the L-mode EMIC instability dominates over the mirror instability [*Shoji et al.*, 2009]. To obtain clear magnetic structures excited by the mirror instability, we perform the hybrid simulations with open boundaries. In the open boundary models, the L-mode EMIC waves go out from the simulation space. On the other hand, the frequency of the mirror-mode structures is zero, and thus they do not propagate away from the place where they arise. Therefore, only the mirror-mode structures remain in the open boundary model. We performed both 2D and 3D hybrid simulations with the open boundaries and compared the mirror-mode structures in these models. The grid spacing Δx is 1.0 V_A/Ω_H (=1.0 c/ω_{pH}), where c and ω_{pH} are the speed of light and the plasma frequency of the proton, respectively. The numbers of grid points are (n_x, n_y, n_z) = (512, 512, 1) and (512, 512, 512) for

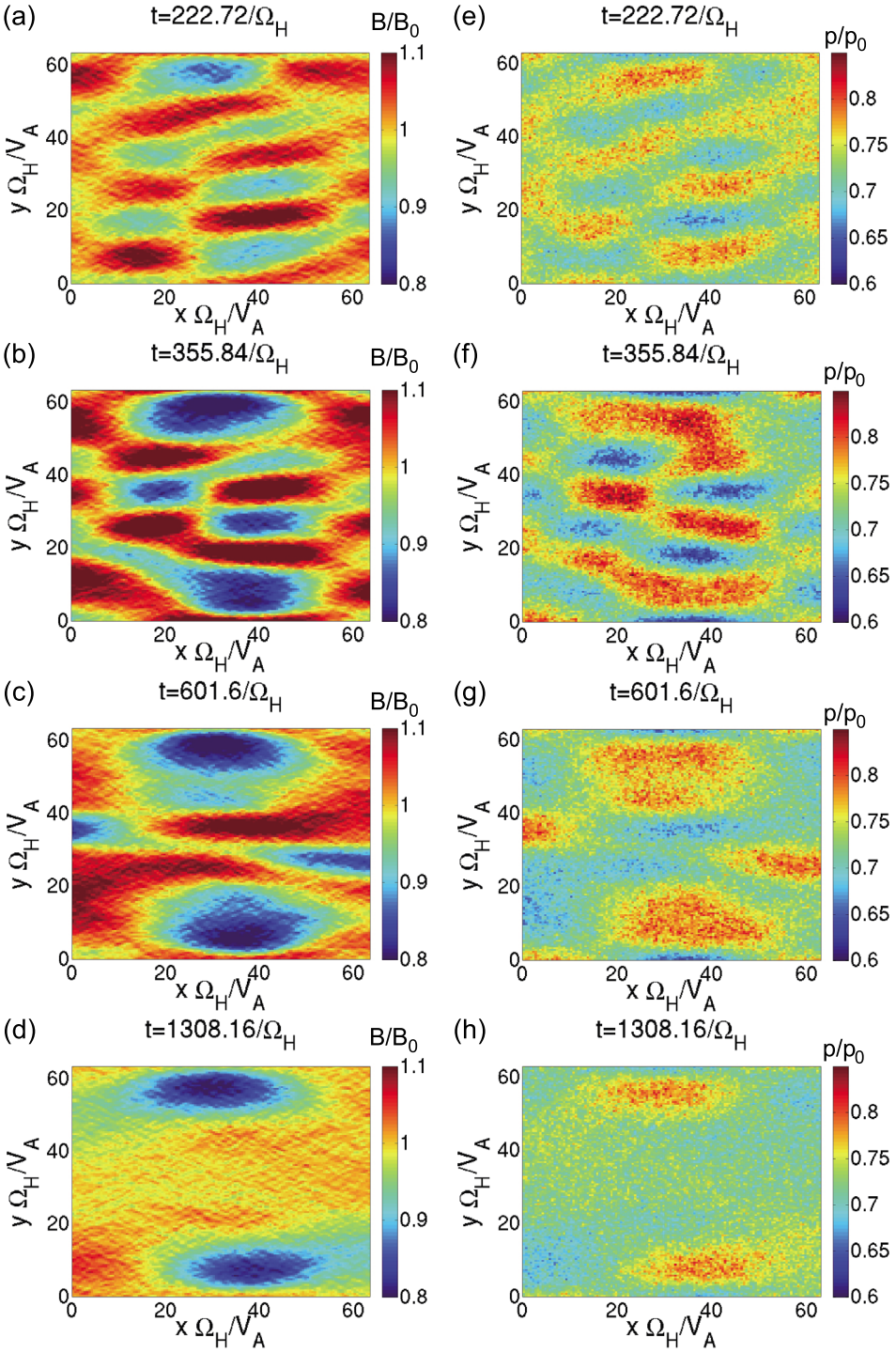

Figure 4. Spatial profiles of the magnetic field $B/B_0 = |\boldsymbol{B}_0 + \delta\boldsymbol{B}|/B_0$ at (a) $t = 222.72/\Omega_H$, (b) $t = 355.84/\Omega_H$, (c) $t = 601.6/\Omega_H$, and (d) $t = 1308.16/\Omega_H$ in the 2D model with $\beta_{||} = 1$. The time evolution of the ion pressure at (e) $t = 222.72/\Omega_H$, (f) $t = 355.84/\Omega_H$, (g) $t = 601.6/\Omega_H$, and (h) $t = 1308.16/\Omega_H$, where $p_0 = B_0^2/2$.

the 2D and 3D models, respectively. The time step is $\Delta t = 0.04/\Omega_H$. The number of superparticles is $N_p = 2^{31}$ in both models.

[9] The 2D open boundary results with the temperature anisotropy $T_\perp/T_{||} = 4$ and the ion beta $\beta_{||} = 0.5$ are shown in Figure 1. The time evolution of the skewness of B_x is shown in Figure 1a. The skewness turns from positive to negative as *Califano et al.* [2008] discussed. As the time increases, the absolute value of the skewness becomes larger. This indicates that the magnetic dips sustain and grow solitary in the 2D model. We find large and clear magnetic dips in Figure 1b, which shows the magnetic field amplitude at $t = 120/\Omega_H$ (shown by the dashed line in Figure 1). The depth of the magnetic dips is ~0.5 B_0. The waveforms in

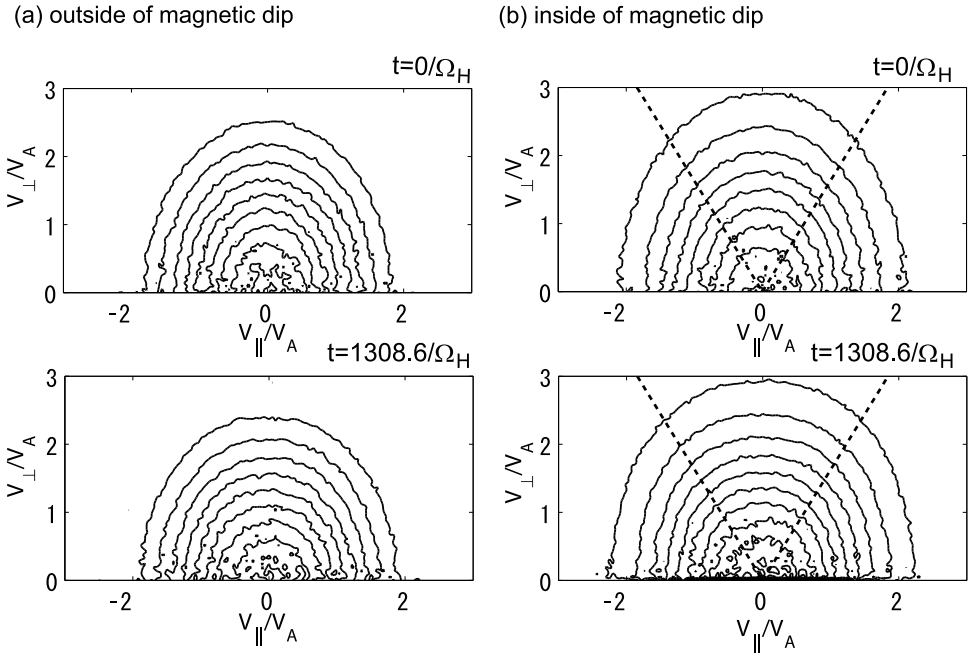

Figure 5. Velocity distribution functions of protons in the 2D local regions (a) inside and (b) outside the dip. The black dashed lines in Figure 5b show the pitch angle $\sin^{-1}\sqrt{(B_{\mathrm{dip}}/B_{\mathrm{out}})}$, and $\pi - \sin^{-1}\sqrt{(B_{\mathrm{dip}}/B_{\mathrm{out}})}$.

the x and y directions are shown in Figures 1d and 1c, respectively. The scale of the magnetic dip in the x direction is larger than that in the y direction. At this time, because of the open boundary effect, the L-mode EMIC waves have already disappeared from the simulation space and we obtain clear magnetic structures of the mirror mode which only persists in the box (no propagation). The variations of the perpendicular components B_y and B_z are much smaller than that of the parallel component B_x. This means the magnetic dips formed by the mirror instability are mostly the parallel component. Because of the condition $\nabla \cdot \boldsymbol{B} = 0$, the components of the magnetic field in the y and z directions exist although they are small. The angular change in the magnetic dip in the 2D model is ~8°. *Tsurutani et al.* [2011] indicates that the magnetic decreases have larger angular change and the magnetic decreases which have the angular change <10° are called "linear magnetic decreases" [*Winterhalter et al.*, 1994]. Thus, the magnetic dips formed by the mirror instability can correspond to "linear magnetic decreases" as mentioned in the previous studies [*Winterhalter et al.*, 1994; *Tsurutani et al.*, 1999b; *Zhang et al.*, 2009].

[10] The 3D open boundary results with the same temperature anisotropy and ion beta as the 2D simulation are shown in Figure 2. The skewness of B_x is always positive as shown in Figure 2a. The skewness has the maximum value at $t = 22/\Omega_H$ which is around the time when the mirror instability stops growing [*Shoji et al.*, 2009]. After the wave growth, coalescence of the mirror mode takes place [*Shoji et al.*, 2009], and the magnetic structure becomes larger. The skewness becomes smaller after $t = 22/\Omega_H$, resulting from depression of the magnetic peaks. Since the magnetic structure collapses finally due to the coalescence, the skewness approaches 0. A more precise analysis between the coalescence and the magnetic structures is given in section 4. Figures 2b and 2c show cross sections of the magnetic field at $t = 22/\Omega_H$ in xz and xy planes, respectively. Variations of the x, y, and z components of the magnetic field vector are plotted as functions of x, y, and z over the ranges including the magnetic peak structure in Figures 2d, 2e, and 2f, respectively. The magnetic peaks are also found only in the x component (in black) of the magnetic field. The mirror instability saturates around $t = 40/\Omega_H$ faster than in the 2D model [*Shoji et al.*, 2009]. It corresponds to the change of the temporal stages of the decreasing skewness as

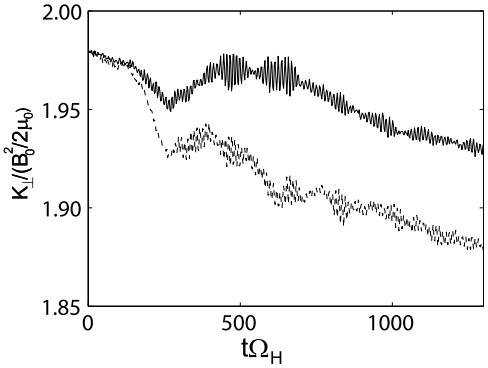

Figure 6. Kinetic energies of the protons in the perpendicular directions inside (solid line) and outside (dashed line) the magnetic dip in the 2D model with $\beta_{\parallel} = 1$.

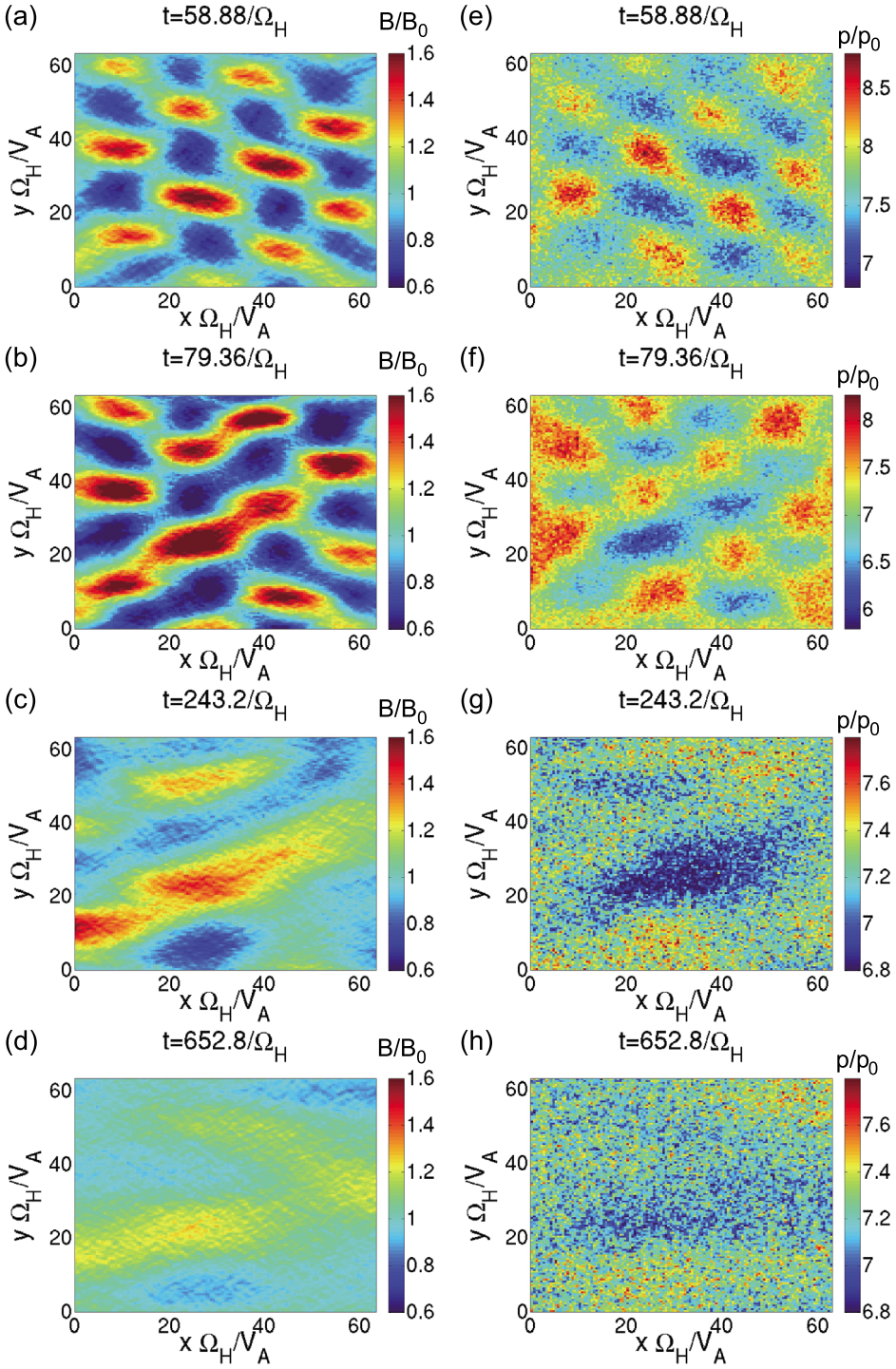

Figure 7. Spatial profiles of the magnetic field $|B_0 + B|$ at (a) $t = 58.88/\Omega_H$, (b) $t = 79.36/\Omega_H$, (c) $t = 245.2/\Omega_H$, and (d) $t = 652.8/\Omega_H$ in the 2D model with $\beta_{||} = 10$. The time evolution of the ion pressure at (e) $t = 58.88/\Omega_H$, (f) $t = 79.36/\Omega_H$, (g) $t = 245.2/\Omega_H$, and (h) $t = 652.8/\Omega_H$ in the 2D model, where $p_0 = B_0^2/2$.

shown in Figure 2a. A more precise study of the time evolution of the skewness is left as a future study.

4. Higher Resolution Simulation for Mirror-Mode Structures

[11] In order to analyze the magnetic structures more precisely, we performed 2D and 3D simulations in small size simulation boxes with higher spatial resolution. The numbers of grids (n_x, n_y, n_z) are (128, 128, 1) and (128, 128, 128) for the 2Dand 3D models, respectively. The grid spacing $\Delta x = 0.5\ \Omega_H / V_A$ (i.e. $0.5\ c/\omega_{pH}$) and the time step $\Delta t = 0.02/\Omega_H$ are used. The number of particles in each grid is assumed as N_p/cell = 2048 and N_p/cell = 128 for the 2D and 3D models, respectively.

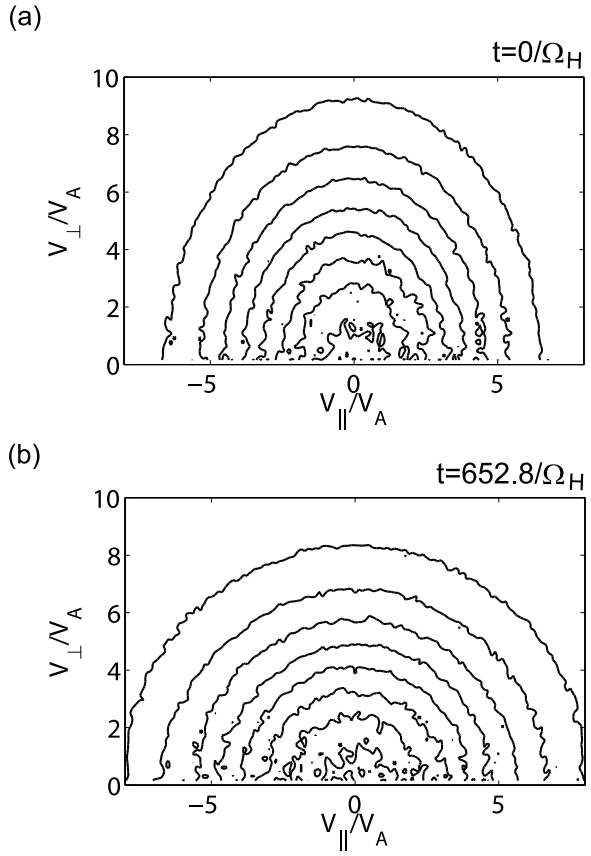

Figure 8. Velocity distribution functions of protons averaged in space in the 2D model in the case with the ion beta $\beta_{\parallel} = 10$ at (a) $t = 0/\Omega_H$ and (b) $t = 652.8/\Omega_H$.

4.1. Magnetic Structures in the 2D Models

[12] Magnetic field structures ($(B_0 + \delta B)/B_0$) generated by a temperature anisotropy $T_{\perp}/T_{\parallel} = 2$ with different parallel betas $\beta_{\parallel} = 1$, 4, and 10 in the 2D model are shown in the right panel of Figures 3a, 3b, and 3c, respectively. The skewness of B_x of each case is also shown in the left panel. We can find the magnetic dips in the right panel of Figure 3a at $t = 1308.6/\Omega_H$. The scale size in the parallel direction ($\sim$20 ion gyroradius) is larger than that in the perpendicular direction ($\sim$10 ion gyroradius). The skewness shown in the left panel of Figure 3a becomes negative within the whole time of concern. This result agrees with that in Figure 1. On the other hand, in the right panels of Figures 3b and 3c, which show the magnetic field at $t = 652.8/\Omega_H$, we find that the magnetic peaks exist dominantly. The left panels of Figures 3b and 3c show that each skewness becomes positive in the later stage. The left panel of Figure 3b shows the skewness temporally turns negative in the later stage. This is because the magnetic peaks go outside slowly through the coalescence and diffusion of the structures, and there still remain magnetic dips around $20 < \tilde{X} < 40$, $0 < \tilde{Y} < 10$, where $\tilde{X} = x\Omega_H/V_A$ and $\tilde{Y} = y\Omega_H/V_A$. This trend, that the magnetic peaks appear instead of the magnetic dips as the parallel component of the ion beta becomes larger, shows a good agreement with the observation results [*Soucek et al.*, 2008].

[13] The time history of the generation processes of the magnetic dips with $\beta_{\parallel} = 1$ is shown in Figures 4a, 4b, 4c, and 4d. The time evolution of the skewness shown in the left panel of Figure 3a indicates that the magnetic dip is dominant. We also show the perpendicular component of the ion pressure $p_{\perp}$ in Figures 4e, 4f, 4g, and 4h, where $p_0 = B_0^2/2$. Because of the pressure balance condition of the mirror instability [*Kivelson and Southwood*, 1996], the ion pressure becomes larger where the magnetic field is weak and vice versa. Because the initial condition of the plasma ($\beta_{\parallel} = 1$ and $T_{\perp}/T_{\parallel} = 2$) is near the threshold of the mirror instability [e.g., *Hasegawa*, 1969]

$$T_{\perp}/T_{\parallel} \simeq 1 + 1/\beta_{\perp}, \tag{2}$$

the mirror instability driven by the temperature anisotropy generates the sinusoidal magnetic structures. The mirror-mode structures have wave vectors almost in the perpendicular angles as shown in Figure 4a due to the linear growth rate. Some particles are trapped inside the region where the magnetic field is weak (magnetic dip), and the ion pressure becomes larger in it as shown in Figure 4e. In Figures 4b and 4c, we find coalescence of some of the magnetic dips, and diffusion of the magnetic peaks. Figures 4f and 4g also indicate the coalescence. In Figures 4d and 4h, we can find that some particles are inside the magnetic dips due to magnetic trapping and thus the pressure becomes larger. The trapping of the protons has been shown in *Pokhotelov et al.* [2008, 2010]. They have discussed the role of the trapped particles in the nonlinear mirror-mode structures.

[14] The velocity distribution function of the protons in these localized regions is also shown in Figure 5. The regions inside and outside the magnetic dip are defined as $16 < \tilde{X} < 48$, $0 < \tilde{Y} < 16$ and $16 < \tilde{X} < 48$, $16 < \tilde{Y} < 32$, respectively in Figures 4d to 4h. The top panels show the initial distributions. A top-flatted velocity distribution function is found in the lower panel of Figure 5b. This is due to the mirror motion of the protons trapped by the magnetic dips. The magnetic structures become like a magnetic mirror device. When a pitch angle α of a proton satisfies

$$\sin^{-1}\sqrt{(B_{\rm dip}/B_{\rm out})} < \alpha < \pi - \sin^{-1}\sqrt{(B_{\rm dip}/B_{\rm out})}, \tag{3}$$

where $B_{\rm out}$ and $B_{\rm dip}$ are amplitudes outside and inside of the magnetic dip, respectively, the proton is trapped in the magnetic mirror structure. We plot the angle $\sin^{-1}\sqrt{(B_{\rm dip}/B_{\rm out})}$ and $\pi - \sin^{-1}\sqrt{(B_{\rm dip}/B_{\rm out})}$ in Figure 5b and find the top-flat velocity structures inside the region satisfying (3). The formation process of the top-flat velocity distribution function has been theoretically driven by *Pokhotelov et al.* [2008, 2010]. The distribution function inside the magnetic dip shows a good agreement with these theoretical results. The pitch angle of these particles are well scattered through this motion and thus the distribution becomes top-flat. Therefore the pressure inside the magnetic dips becomes larger as shown in Figure 6. The proton distribution functions outside the dip shown in the lower panel of the Figure 5a, on the other hand, do not have such a top-flat structure. Because the

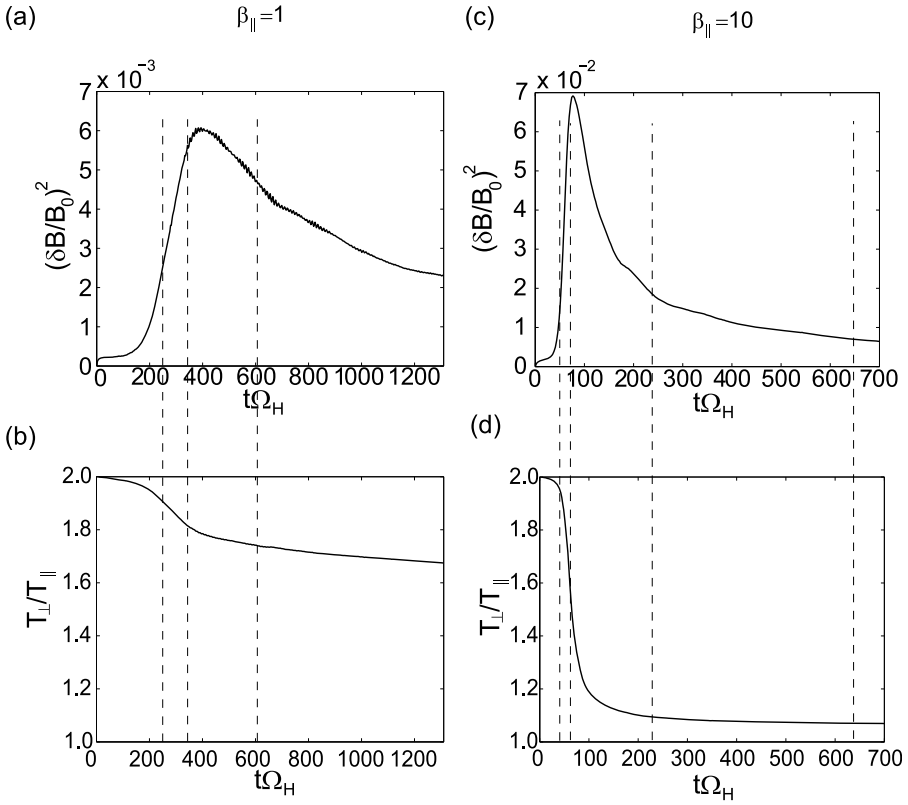

Figure 9. Time histories of magnetic field energies and temperature anisotropies for (a and b) $\beta_{\parallel} = 1$ and for (c and d) $\beta_{\parallel} = 10$ in the 2D models. Dashed lines correspond to the times of the panels of the spatial profile in Figures 4 and 7.

mirror instability starts from the low beta condition near the threshold of the instability, the particles are less heated.

[15] THEMIS observation [*Balikhin et al.*, 2009] shows that the evolution of perpendicular temperature inside the magnetic dip increases as magnetic field decreases within the dip. *Balikhin et al.* [2009] explain this as the evidence of the macro-effects of the particles trapped inside the magnetic dips. Since a number of the particles are trapped and the adiabatic invariant μ is conserved, the perpendicular temperature $T_{\perp}$ inside the dip should become larger than that outside the dip. We calculate the localized kinetic energy of the protons in the perpendicular directions both inside and outside the magnetic dips in Figure 6, which show an agreement with the THEMIS observation. Since the trapped particles inside the magnetic dip have larger pitch angles than those outside the dip, the perpendicular energy is larger than the parallel energy in the later stage.

[16] The time evolutions of magnetic structures and ion pressures in the perpendicular direction in the case of $\beta_{\parallel} = 10$ are shown in Figures 7a and 7b, respectively. Since the initial condition of the protons ($\beta_{\parallel} = 10$ and $T_{\perp}/T_{\parallel} = 2$) is far from the threshold of the mirror instability

$$T_{\perp}/T_{\parallel} \gg 1 + 1/\beta_{\perp}, \tag{4}$$

according to the linear growth theory, the mirror-mode structures are initially driven with larger wave vectors in oblique angles as we can see in the top panel of Figure 7a. Through Figures 7a to 7d and Figures 7e to 7h, we find coalescences of magnetic structures [*Shoji et al.*, 2009] and the associated pressure of ions, respectively. After the coalescence, the magnetic dips almost disappear as shown in Figure 7d. Strong diffusion of magnetic structures can be found through the coalescence. The skewness of this case is shown in the left panel of Figure 3c. At an early stage, both the magnetic peaks and dips exist and thus the skewness changes rapidly. Due to the diffusion of the magnetic structures, the skewness becomes smaller at later stage. However, they do not turn to the negative value, i.e. the magnetic dips do not appear dominantly.

[17] In Figure 8, we show the distribution functions averaged in space in the case with $\beta_{\parallel} = 10$. There is little difference between the distribution functions inside and outside the magnetic peaks since the particle trapping do not take place after the magnetic peaks appear as we can see in Figure 7h. The upper panel of Figure 8 shows the initial distribution function. After the magnetic peak is generated, shown in the lower panel of Figure 8, the distribution function becomes larger in the parallel direction. In the growing phase of the mirror instability, the mirror-mode structures have the electric field in the parallel direction because they are caused by the oblique wave numbers. The wave amplitude becomes larger in Figure 7a than that in Figure 4a because of the larger initial growth rate. At the growth phase, the electric fields

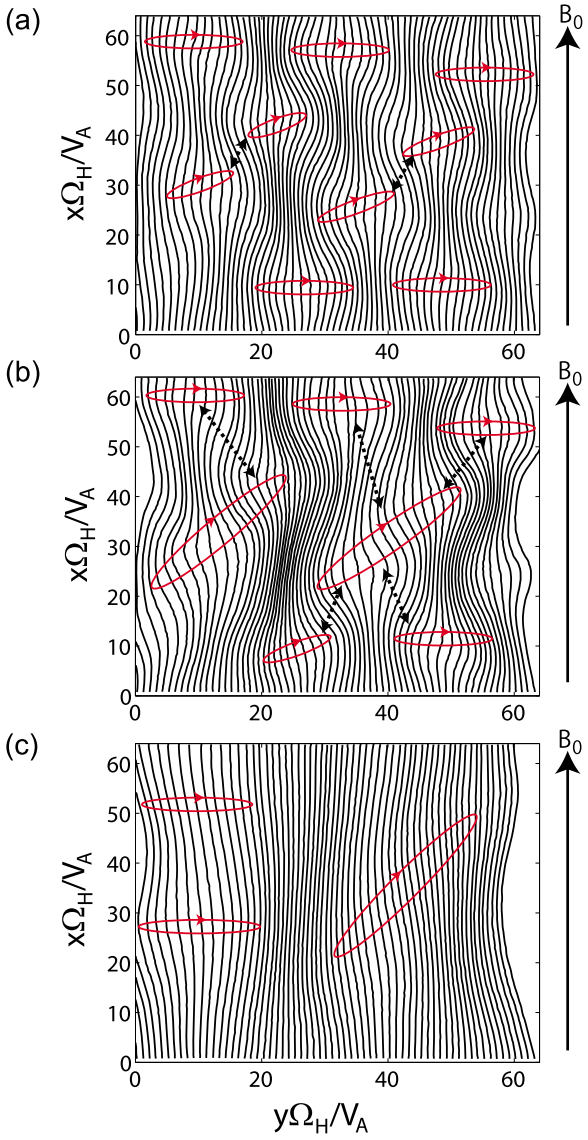

Figure 10. Spatial profiles of the magnetic field line (black lines) in the 2D model with $\beta_{||} = 10$ at (a) $t = 58.88/\Omega_H$, (b) $t = 79.36/\Omega_H$, and (c) $t = 245.2/\Omega_H$, and the schematic plots of the diamagnetic currents which reduces the magnetic field density inside the magnetic dip regions (red lines). The attractive force between the current loops leads to coalescence of neighboring magnetic structures.

of the mirror instability are generated strongly since the magnetic field changes in time, and thus the perpendicular energy of the protons is transferred into the parallel direction both inside and outside the magnetic peaks as shown in the lower panel of Figure 8.

[18] Figures 9a and 9c show the time evolutions of the magnetic energies in the cases of $\beta_{||} = 1$ and $\beta_{||} = 10$, respectively. Figures 9b and 9d show the time evolutions of the temperature anisotropies in these 2D models. In the lower beta case, the growth of the magnetic energy stops around $T_\perp/T_{||} \sim 1.8$ since it reaches the marginal stable. The magnetic energy decreases in the nonlinear stage although the amplitude of the magnetic dips does not change. This is because the magnetic structures go out from the simulation space slowly as we can find in Figures 4b to 4d. In the high beta case, on the other hand, the energy transfer of the particles resulting in the strong diffusion of the magnetic peaks can be also found in Figures 9c and 9d. After the coalescence starts ($t \sim 58.88/\Omega_H$), the temperature anisotropy starts to decrease quickly. After the linear growth finishes around $t \sim 100/\Omega_H$ in Figure 9c, the magnetic energy becomes smaller due to the currents caused by the coalescence. Compared with Figure 9c, the temperature anisotropy in the high beta model becomes much smaller than in the low beta model. This also indicates the particle energy transfer into the parallel direction in the high beta condition. The currents diffusing the magnetic structures are discussed in the next paragraph.

[19] These results indicate that the magnetic peaks in the 2D models are formed through the following processes. The temperature anisotropy of the protons excites the mirror instability far above the threshold. The generated mirror-mode structures form sinusoidal mesh structures as shown in Figure 7a. At the same time, the protons have larger parallel velocity due to the growing mirror-mode structures and thus the protons gain higher mobility. The magnetic field lines at this time are shown in Figure 10a. In the magnetic dips, there appear "ion bubbles", which consist of the trapped ions inside the magnetic dips as shown in Figure 7e. The schematic plots of diamagnetic currents (red lines) inside the magnetic dips are also shown. The neighboring current loops attract with each other and thus, these currents merge. As a result, the coalescence of the ion bubbles in the magnetic dips takes place. The coalesced magnetic dips form "magnetic troughs" as shown in Figure 7b. The magnetic field lines are shown in Figure 10b. The magnetic troughs are supported by the merged current lines. As the coalescence proceeds further, the troughs become larger. The regions with larger magnetic fields remain between the magnetic troughs, appearing as the magnetic peaks as shown in Figures 7c and 10c. Since the particles with high mobility have large velocities, they easily go across the magnetic structures causing the diamagnetized current. Thus the high mobility of the particles helps the continuous coalescence. These particles also move across the magnetic peaks, and thus the magnetic peaks diffuse as shown in Figure 7d.

4.2. Magnetic Structures in the 3D Models

[20] The right panels of Figures 11a, 11b, and 11c show cross sections of $B = |\boldsymbol{B}_0 + \delta\boldsymbol{B}|$ in the 3D model with the temperature anisotropy $T_\perp/T_{||} = 2$ and the ion beta $\beta_{||} = 1$ (at $t = 164/\Omega_H$), $\beta_{||} = 4$ (at $t = 164/\Omega_H$) and $\beta_{||} = 10$ (at $t = 92.25/\Omega_H$), respectively. The background magnetic field $\boldsymbol{B}_0$ is along the x direction. We find magnetic peaks structures in each case of the 3D simulation (skewness of B_x is always positive in each left hand panel), although we use the same plasma parameters as in 2D models.

[21] In order to clarify this result, we plot the magnetic field and the density of protons respectively in Figures 12a and 12b at different times of the simulation, with the ion beta $\beta_{||} = 10$ and the temperature anisotropy $T_\perp/T_{||} = 2$. The top panel of Figure 12a shows the configuration of the mirror-mode structures at a time corresponding to the linear growth phase. Through the middle and bottom panels of

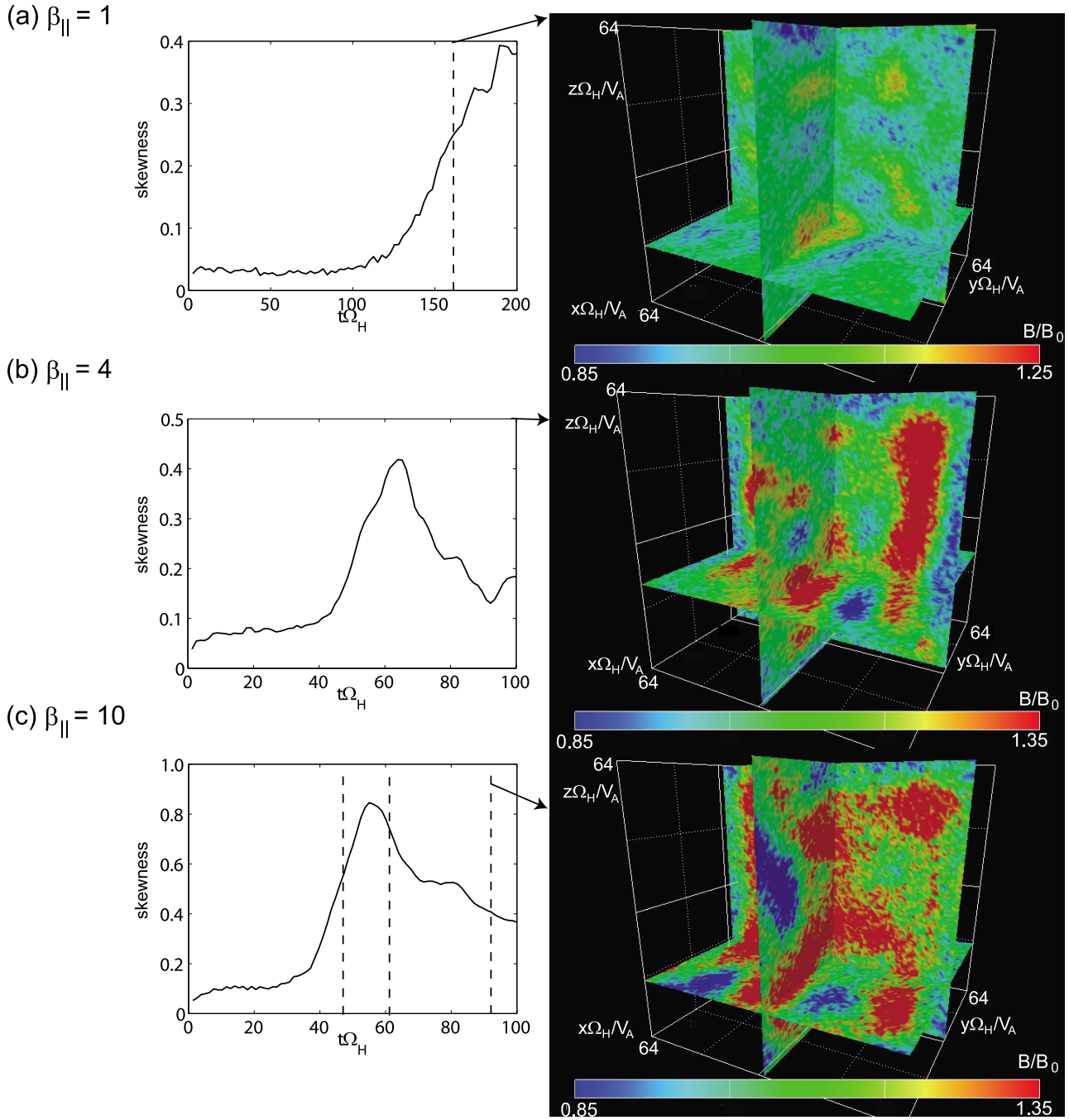

Figure 11. (left) Skewness of B_x and (right) Magnetic field in the 3D models with the initial ion parameters $T_\perp/T_\parallel = 2$ and (a) $\beta_\parallel = 1$ at $t = 164/\Omega_H$ (b) $\beta_\parallel = 4$ $t = 164/\Omega_H$, and (c) $\beta_\parallel = 10$ $t = 92.25/\Omega_H$.

Figure 12a, we clearly find the coalescence of magnetic structures. On the other hand, in the top panel of Figure 12b, we find the density enhanced due to the diamagnetism in the mirror-mode structures. Because of the increase of the degree of freedom in the perpendicular direction, there exist more neighbor magnetic dips (bubbles) than in the 2D model. As a result the merging of the diamagnetic currents takes place in these neighboring dips. As the mirror-mode structures coalesce, the magnetic peaks appear similar to those in Figure 10. In Figure 12b, as the time proceeds, the density becomes larger around the magnetic peaks.

[22] Figures 13a and 13b show the time evolution of the magnetic energy density and the temperature anisotropy of the protons. Times t_1, t_2, and t_3 correspond to the times of the top, middle and bottom panels of Figure 12, respectively. The evolution in the range of $0 < t < t_1$ is associated with the fast generation of the EMIC instability with the larger initial growth rate. The magnetic energy becomes slightly larger

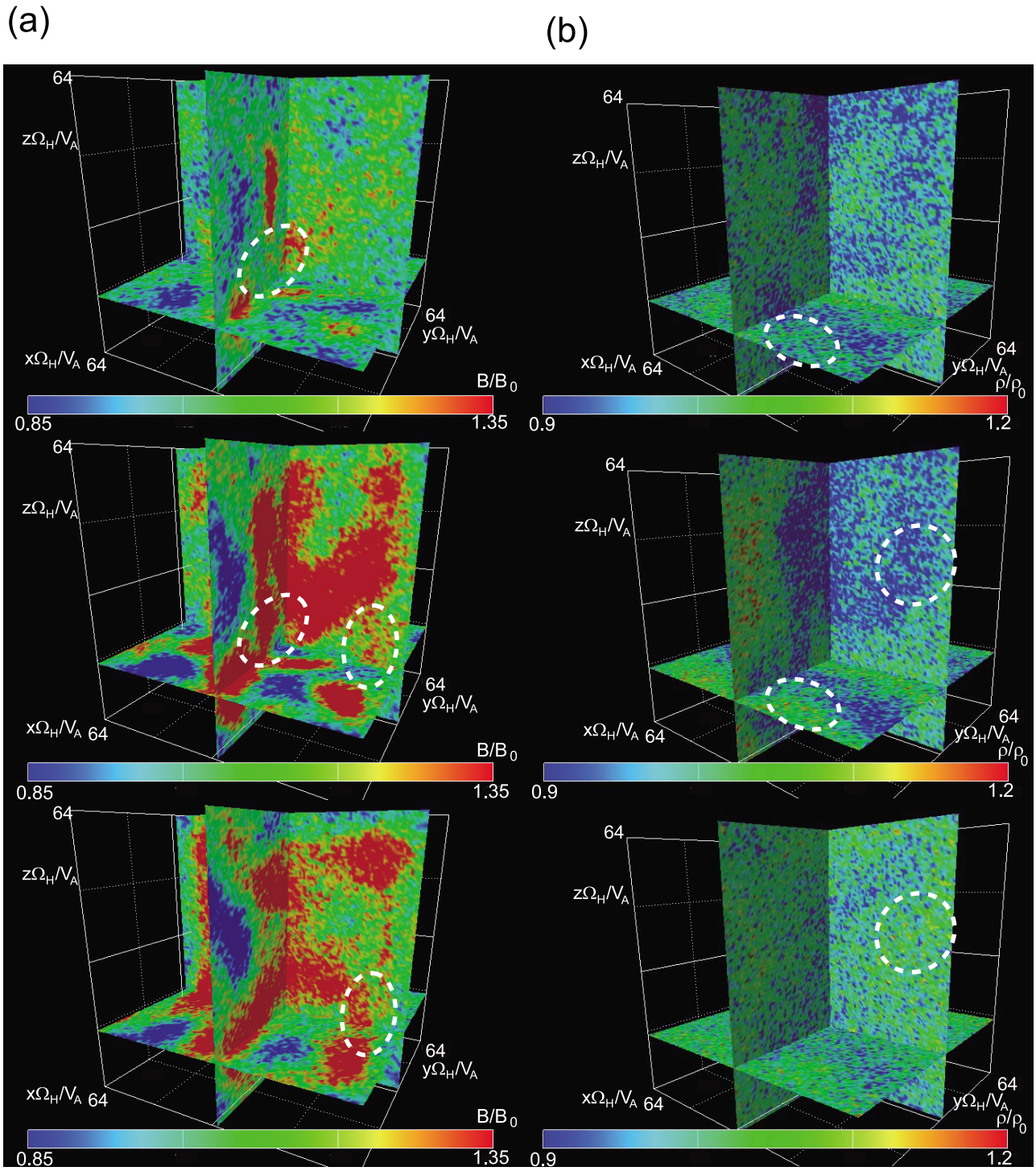

Figure 12. Cross sections of the 3D structures of the (a) the magnetic field B and (b) density ρ_i with $\beta_{||} = 10$. The top, middle, and bottom panels show the values at $t = 41/\Omega_H$, $t = 61.5/\Omega_H$, and $t = 92.25/\Omega_H$, respectively. White dashed circles show the region where the coalescence takes place in the magnetic field (Figure 12a) and where the ion density increases (Figure 12b). The ion density is large at locations where the magnetic field is weak and vice versa (similarly to Figures 7a and 7b for 2D simulations).

while the temperature anisotropies of the particles are relaxed at the same time as shown in Figure 13b. In $t_1 < t < t_2$, the mirror instability grows dominantly, because the mirror-mode structures stay in the system, while the temperature anisotropy is relaxed rapidly. After the saturation, $t > t_2$, the magnetic energy starts to decrease due to the particle heating during the coalescences of the magnetic structures as shown in Figure 7d. Because of the heating, the temperature anisotropy also keeps decreasing. As the magnetic peaks are generated, the magnetic field

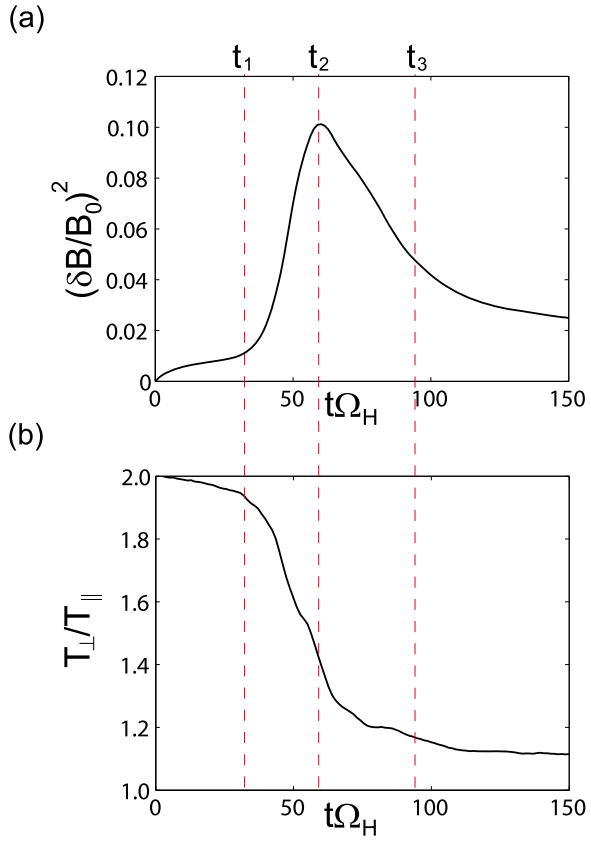

Figure 13. Time history of the (a) magnetic energy density and (b) temperature anisotropy in the 3D models. Times $t_1 = 41/\Omega_H$, $t_2 = 61.5/\Omega_H$, and $t_3 = 92.25/\Omega_H$ correspond to the times of the top, middle, and bottom panels of Figure 12.

outside the magnetic peaks become smaller as we can see in Figure 12.

5. Summary of Simulations and Comparison With Observations

[23] We have compared the magnetic structures generated by the nonlinear evolution of the mirror instability between the 2D and 3D open boundary models. In the 2D model, fine structures of the magnetic dips are locally generated. On the other hand, in the 3D system, the magnetic peaks are found in the localized regions. These magnetic structures mainly have parallel component B_x. We also performed the small size simulations with higher spatial resolution both in the 2D and 3D models with various ion beta values. We only find the magnetic dips in the 2D model with the low ion beta ($\beta_{\|} \lesssim 1$). For other cases, the magnetic peaks appear. In the 3D model, we obtain the magnetic peak structures as shown in Figures 11. We summarize the simulation results in Table 1. Compared with the 2D results, the timescales become faster in the 3D model, because more modes consume the free energy of the temperature anisotropy faster [*Shoji et al.*, 2009]. The timescale in the high beta conditions also becomes faster than that in the low beta condition since the linear growth rate becomes larger as the ion beta becomes larger. In the high beta condition, the ions have larger thermal velocities. Therefore, some of them have large velocity and thus they have large mobility supporting continuous coalescence.

[24] The mirror instability has the maximum growth rate in the higher wave numbers (smaller wavelength) with the lower initial ion beta. In the lower initial ion beta $\beta_{\|} = (V_{th\|}/V_A)^2$ condition most of the thermal particles have small parallel velocities. Some particles with larger pitch angles are trapped by the magnetic structures. Because the magnetic structures are uniform in the z direction in the 2D models, they are easily trapped in the area with decreased magnetic field compared with those in the 3D models. Thus, the magnetic dips appear in the 2D models. In the higher ion beta cases, on the other hand, because of the stronger pitch angle scattering into the parallel direction and the large initial parallel velocities, the number of the particles which can be trapped by the magnetic structures become smaller. The coalescence of the magnetic dips takes place in both low and high beta cases. The coalescence is explained by the attraction of the diamagnetic current loops inside the magnetic dips (bubbles) as shown in Figure 10. Since the coalescence rate becomes larger as the mobility of the particles trapped inside the dips becomes larger, the current loops merge effectively in the high beta cases. The recent observation study [*Balikhin et al.*, 2010] indicates that the magnetic peaks are observed as "walls" between "huge magnetic dips". The continuous coalescence results in the "huge magnetic dips" corresponding to the observations.

[25] The magnetic dips are observed near the magnetopause rather than near the bowshock [*Soucek et al.*, 2008]. The simulation result that the magnetic dips are generated only in the 2D model of the low ion beta condition indicates the possibility that the magnetosheath near the magnetopause has a 2D spatial configuration for the mirror-mode structure. Because of the existence of the magnetopause which works as a magnetic obstacle, the wave number vector in the normal direction to the magnetopause is restricted. Since the magnetic field becomes larger near the magnetopause, the ion beta becomes smaller. Thus, the region near the

Table 1. Summary of Parametric Analyses of the Magnetic Structures[a]

	2D With Low Beta	2D With High Beta	3D With Low Beta	3D With High Beta
τ_s	$\sim 400/\Omega_H$	$\sim 100/\Omega_H$	$\sim 170/\Omega_H$	$\sim 60/\Omega_H$
B_w	$\sim 0.2\ B_0$	$\sim 0.8\ B_0$	$\sim 0.25\ B_0$	$\sim 0.35\ B_0$
τ_n	$\sim 1200/\Omega_H$	$\sim 240/\Omega_H$	$\sim 200/\Omega_H$	$\sim 90/\Omega_H$
Ion mobility	low (trapped)	high	high	high
Coalescence	weak	strong	strong	strong
Structure	magnetic dip	magnetic peak	magnetic peak	magnetic peak

[a]Saturation time, maximum wave amplitude, and timescale of formation of nonlinear magnetic structures are indicated by τ_s, B_w, and τ_n, respectively.

magnetopause becomes similar to the 2D model with low beta condition. In other regions of the magnetosheath far away from the magnetopause, the spatial configuration becomes 3D, and the magnetic peaks are observed dominantly. The temperature anisotropy also changes through the bowshock to the magnetopause and this analysis is left for a future study.

[26] **Acknowledgments.** Computation in the present study was performed with the KDK system of Research Institute for Sustainable Humanosphere (RISH) and Academic Center for Computing and Media Studies at Kyoto University as a collaborative research project. The present study was supported in part by Grant-in-Aid for Research Fellows from the Japan Society for the Promotion of Science (JSPS), Grant-in-Aid 23340147 of the Ministry of Education, Science, Sports and Culture of Japan, and by the National Science Council in Taiwan.

[27] Philippa Browning thanks the reviewers for their assistance in evaluating this paper.

References

Balikhin, M. A., R. Z. Sagdeev, S. N. Walker, O. A. Pokhotelov, D. G. Sibeck, N. Beloff, and G. Dudnikova (2009), THEMIS observations of mirror structures: Magnetic holes and instability threshold, *Geophys. Res. Lett.*, *36*, L03105, doi:10.1029/2008GL036923.

Balikhin, M. A., O. A. Pokhotelov, S. N. Walker, R. J. Boynton, and N. Beloff (2010), Mirror mode peaks: THEMIS observations versus theories, *Geophys. Res. Lett.*, *37*, L05104, doi:10.1029/2009GL042090.

Birdsall, C. K., and A. B. Langdon (1985), *Plasma Physics Via Computer Simulation*, McGraw-Hill, New York.

Califano, F., P. Hellinger, T. Passot, P. L. Sulem, and P. Travnicek (2008), Nonlinear mirror mode dynamics: Simulations and modeling, *J. Geophys. Res.*, *113*, A08219, doi:10.1029/2007JA012898.

Chandrasekhar, S. A., A. N. Kaufman, and K. M. Watson (1958), The stability of the pinch, *Proc. R. Soc. London Ser. A*, *245*, 435.

Gary, S. P. (1992), The mirror and ion cyclotron anisotropy instabilities, *J. Geophys. Res.*, *97*, 8519.

Glassmeier, K. H., P. N. Mager, and D. Y. Klimushkin (2003), Concerning ULF pulsations in Mercury's magnetosphere, *Geophys. Res. Lett.*, *30* (18), 1928, doi:10.1029/2003GL017175.

Hasegawa, A. (1969), Drift mirror instability in the magnetosphere, *Phys. Fluids*, *12*, 2642.

Hasegawa, A. (1975), *Plasma Instabilities and Nonlinear Effects*, *Phys. Chem. Space*, vol. 8, 94 pp., Springer, New York.

Hellinger, P., P. Travnicek, J. C. Kasper, and A. J. Lazarus (2006), Solar wind proton temperature anisotropy: Linear theory and WIND/SWE observations, *Geophys. Res. Lett.*, *33*, L09101, doi:10.1029/2006GL025925.

Hubert, D. (1994), Nature and origin of wave modes in the dayside Earth magnetosheath, *Adv. Space Res.*, *14*(7), 55.

Kennel, C. F., and H. E. Petschek (1966), Limit on stably trapped particle fluxes, *J. Geophys. Res.*, *71*, 1.

Kivelson, M. G., and D. J. Southwood (1996), Mirror instability II: The mechanism of nonlinear saturation, *J. Geophys. Res.*, *101*, 17,365.

Lacombe, C., and G. Belmont (1995), Waves in the Earth's magnetosheath: Observations and interpretations, *Adv. Space Res.*, *15*(8/9), 329.

Lee, L., C. Price, C. Wu, and M. Mandt (1988), A study of mirror waves generated downstream of a quasi perpendicular shock, *J. Geophys. Res.*, *93*, 247.

Matsumoto, H., and Y. Omura (1993), *Computer Space Plasma Physics*, Terra Sci. Publ., Tokyo.

Omura, Y., H. Usui, and H. Matsumoto (1988), Parallel heating associated with interaction of forward and backward electromagnetic cyclotron waves, *J. Geomag. Geoelectr.*, *40*, 949.

Phan, T. D., G. Paschmann, W. Baumjohann, N. Sckopke, and H. Luhr (1994), The magnetosheath region adjacent to the dayside magnetopause: AMPTE/IRM observations, *J. Geophys. Res.*, *99*, 121.

Pokhotelov, O. A., R. Z. Sagdeev, M. A. Balikhin, and R. A. Treumann (2004), Mirror instability at finite ion-Larmor radius wavelengths, *J. Geophys. Res.*, *109*, A09213, doi:10.1029/2004JA010568.

Pokhotelov, O. A., R. Z. Sagdeev, M. A. Balikhin, O. G. Onishchenko, and V. N. Fedun (2008), Nonlinear mirror waves in non-Maxwellian space plasmas, *J. Geophys. Res.*, *113*, A09213, doi:10.1029/2004JA010568.

Pokhotelov, O. A., Sagdeev, R. Z., Balikhin, M. A., Fedun, V. N., and Dudnikova, G. I. (2010), Nonlinear mirror and Weibel modes: Peculiarities of quasi-linear dynamics, *Ann. Geophys.*, *28*, 2161.

Price, C., D. Swift, and L. C. Lee (1986), Numerical simulation of non-oscillatory mirror waves at the Earth's magnetosheath, *J. Geophys. Res.*, *91*, 101.

Russell, C. T., P. Song, and R. P. Lepping (1989), The Uranian magnetopause: Lessons from Earth, *Geophys. Res. Lett.*, *16*, 1485.

Shoji, M. and Y. Omura (2011), Simulation of Electromagnetic Ion Cyclotron Triggered Emissions in the Inner Magnetosphere, *J. Geophys. Res.*, *116*, A05212, doi:10.1029/2010JA016351.

Shoji, M., Y. Omura, B. T. Tsurutani, O. P. Verkhoglyadova, and B. Lembege (2009), Mirror instability and L-mode electromagnetic ion cyclotron instability: Competition in the Earth's magnetosheath, *J. Geophys. Res.*, *114*, A10203, doi:10.1029/2008JA014038.

Shoji, M., Y. Omura, B. Grison, J. Pickett, and I. Dandouras (2011), Electromagnetic ion cyclotron waves in the helium branch induced by multiple electromagnetic ion cyclotron triggered emissions, *Geophys. Res. Lett.*, *38*, L17102, doi:10.1029/2011GL048427.

Soucek, J., E. Lucek, and I. Dandouras (2008), Properties of magnetosheath mirror modes observed by Cluster and their response to changes in plasma parameters, *J. Geophys. Res.*, *113*, A04203, doi:10.1029/2007JA012649.

Southwood D. J., and M. G. Kivelson (1993), Mirror instability: 1. Physical mechanism of linear instability, *J. Geophys. Res.*, *98*, 9181.

Tsurutani, B. T., E. J. Smith, R. R. Anderson, K. W. Ogilvie, J. D. Scudder, D. N. Baker, and S. J. Bame (1982), Lion roars and nonoscillatory drift mirror waves in the magnetosheath, *J. Geophys. Res.*, *87*, 6060.

Tsurutani, B. T., I. G. Richaradson, R. P. Lepping, R. D. Zwickl, D. E. Jones, E. J. Smith, and S. J. Bame (1984), Drift mirror mode waves in the distant (x ∼ 200 RE) magnetosheath, *Geophys. Res. Lett.*, *11*, 1102.

Tsurutani, B. T., D. J. Southwood, E. J. Smith, and A. Balogh (1993), A survey of low-frequency (LF) waves at Jupiter: The Ulysses encounter, *J. Geophys. Res.*, *98*, 21,203.

Tsurutani, B. T., G. S. Lakhina, E. J. Smith, B. Buti, S. L. Moses, F. V. Coroniti, A. L. Brinca, J. A. Slavin, and R. D. Zwickl (1999a), Mirror mode structures and ELF plasma waves in the Giacobini-Zinner magnetosheath, *Nonlinear Proc. Geophys.*, *6*, 229.

Tsurutani, B. T., G. S. Lakhina, D. Winterhalter, J. K. Arballo, C. Galvan, and R. Sukurai (1999b), Energetic particle cross-field diffusion: Interaction with Magnetic Decreases (MDs), *Nonlinear Proc. Geophys.*, *6*, 235.

Tsurutani, B. T., G. S. Lakhina, O. P. Verkhoglyadova, E. Echer, F. L. Guarnieri, Y. Narita, and D. O. Constantinescu (2011), Magnetosheath and heliosheath mirror mode structures, interplanetary magnetic decreases, and linear magnetic decreases: Differences and distinguishing features, *J. Geophys. Res.*, *116*, A02103, doi:10.1029/2010JA015913.

Umeda, T., Y. Omura, and H. Matsumoto (2001), An improved masking method for absorbing boundaries in electromagnetic particle simulations, *Comput. Phys. Commun.*, *137*, 286.

Vedenov, A. A., and R. Z. Sagdeev (1958), Some properties of plasma with an anisotropic ion velocity distribution in a magnetic field, in *Plasma Physics and the Problem of Controlled Thermonuclear Reactions*, vol. 3, p. 332, Pergamon, New York.

Violante, L., M. B. Bavassano Cattaneo, G. Moreno, and J. D. Richardson (1995), Observations of mirror mode and plasma depletion layer upstream of Saturn's magnetopause, *J. Geophys. Res.*, *100*, 12,047.

Winterhalter, D., M. Neugebauer, B. Goldstein, E. Smith, S. Bame, and A. Balogh (1994), Ulysses field and plasma observations of magnetic holes in the solar wind and their relation to mirror-mode structures, *J. Geophys. Res.*, *99*, 23,371.

Zhang, T. L. et al. (2009), Mirror mode structures in the solar wind at 0.72 AU, *J. Geophys. Res.*, *114*, A10107, doi:10.1029/2009JA014103.